JOURNAL OF ENDOUROLOGY
Volume 35, Number 6, June 2021

Pp. 860–870
DOI: 10.1089/end.2020.0349

The Role of Cavitation in Energy Delivery and Stone Damage During Laser Lithotripsy

Derek S. Ho, PhD,[1] Dominick Scialabba, BS,[1] Russell S. Terry, MD,[2] Xiaojian Ma, BS,[1,3] Junqin Chen, MS,[1] Georgy N. Sankin, PhD,[1] Gaoming Xiang, PhD,[1] Robert Qi, MD,[2] Glenn M. Preminger, MD,[2] Michael E. Lipkin, MD, MBA,[2] and Pei Zhong, PhD[1]

Abstract

Purpose: Although cavitation during laser lithotripsy (LL) contributes to the Moses effect, the impact of cavitation on stone damage is less clear. Using different laser settings, we investigate the role of cavitation bubbles in energy delivery and stone damage.

Materials and Methods: The role of cavitation in laser energy delivery was characterized by using photodetector measurements synced with high-speed imaging for laser pulses of varying durations. BegoStone samples were treated with the laser fiber oriented perpendicularly in contact with the stone in water or in air to assess the impact of cavitation on crater formation. Crater volume and geometry were quantified by using optical coherence tomography. Further, the role of cavitation in stone damage was elucidated by treatment in water with the fiber oriented parallel to the stone surface and by photoelastic imaging.

Results: Longer pulse durations resulted in higher energy delivery but smaller craters. Stones treated in water resulted in greater volume, wider yet shallower craters compared with those treated in air. Stones treated with the parallel fiber showed crater formation after 15 pulses, confirmed by high-speed imaging of the bubble collapse with the resultant stress field captured by photoelastic imaging.

Conclusions: Despite improved energy delivery, the longer pulse mode produced smaller crater volume, suggesting additional processes secondary to photothermal ablation are involved in stone damage. Our critical observations of the difference in stone damage treated in water *vs* in air, combined with the crater formation by parallel fiber, suggest that cavitation is a contributor to stone damage during LL.

Keywords: laser, lithotripsy, kidney calculi

Introduction

The majority of patients with symptomatic renal and ureteral calculi are currently managed with endourologic techniques. The Holmium (Ho):YAG laser has been the clinical gold standard for intracorporeal laser lithotripsy (LL) over the past two decades.[1] Recent advances in LL technologies offer a variety of treatment modes to improve fragmentation efficiency. In particular, pulse width modulation has been extensively studied as a means to reduce stone retropulsion and fiber burn back but has demonstrated mixed results in stone fragmentation efficiency.[2–5]

Stone fragmentation during long pulse, solid-state Ho:YAG LL has been traditionally described as a photothermal process of laser absorption by the stone leading to ablation, and by water pockets in the stone leading to thermal expansion and mechanical stress fields.[6–9] During LL, absorption of each laser pulse causes rapid vaporization of fluid at the fiber tip, leading to the formation of an elongated vapor channel (i.e., the Moses effect) that has primarily been considered as an efficient means for energy delivery to the stone.[6,10–13]

In this study, we investigate the impact of the LL-generated bubbles on stone fragmentation. The laser pulse duration directly affects the bubble geometry and dynamics, both of which impact ablation mechanisms. For Ho:YAG lasers used in clinical urology, the long pulse duration (>100 μsec) produces an elongated bubble with a weak shockwave emission, which has been presumed to cause negligible damage.[6,14] However, prior work has also demonstrated that the collapse of cavitation bubbles near a solid boundary can produce a water jet toward the solid boundary, which may contribute to stone damage during LL.[6,15–18]

[1]Department of Mechanical Engineering and Materials Science, Duke University, Durham, North Carolina, USA.
[2]Division of Urology, Department of Surgery, Duke University Medical Center, Durham, North Carolina, USA.
[3]Department of Research and Development, China Academy of Launch Vehicle Technology, Beijing, China.

We investigate the possibility of water jet impact from the asymmetric bubble collapse on stone damage during LL with and without the contribution of photothermal ablation. Our results suggest that the current understanding of LL as a dominant photothermal ablation process needs to be augmented by the additional role of LL-generated asymmetric bubble collapse with jet impact as a potential contributing factor to stone damage.

Materials and Methods

Pulse energy analysis in air and in water at 4 mm standoff distance

Three pulse modes of different pulse durations from a clinical holmium laser lithotripter (H Solvo 35-watt laser; Dornier MedTech) were investigated in this study at 0.8 J energy setting: (1) Fragmenting Mode with a full width at half maximum (FWHM) pulse duration $\approx 75\,\mu$sec, (2) Standard Mode—FWHM $\approx 150\,\mu$sec, and (3) Advanced Mode—FWHM $\approx 200\,\mu$sec. All the experiments were conducted with the same laser delivery fiber (Dornier SingleFlex 400, NA = 0.26, 365 μm core diameter, 430 μm fiber diameter). The pulse FWHM were calculated from the temporal pulse power profile measured in air by using an InGaAs photodetector (PDA10D; Thorlabs, Newton, NJ).

Power measurements were additionally collected in water by directing the laser pulse into a light guide (at a standoff distance [SD] of 4 mm) that transmitted the light to the photodetector outside of the water tank (Fig. 1a). These measurements were synced with video images captured by a high-speed camera (Phantom v7.3; Vision Research, Wayne, NJ) operating at 40,000 frames per second to correlate bubble dynamics with resultant energy transmission. Pulse energies were quantified by integrating the raw power profiles over time, and the mean relative pulse energies ($n = 30$) were compared between modes in air and water to determine the effects of the bubble on energy delivery in water. Statistical analysis was performed by using *t*-tests ($\alpha = 0.05$, $p < 0.05$).

Damage assessment of wet BegoStone samples treated in water and in air

The damage efficiency was determined by treating BegoStone samples (BEGO USA, Lincoln, RI), a common kidney stone phantom with similar mechanical properties to human calculi.[19,20] BegoStone samples (50 × 50 mm lateral dimension, 5 mm thickness) were prepared at a 5:2 powder to water ratio and cured on an orbital shaker, and they were subsequently soaked in water for 24 hours before the experiment. This protocol localized air pockets and impurities at the center of the sample, allowing us to carry out stone damage experiments on the uniform peripheral area with minimal voids to improve consistency in damage assessment. The samples were polished to prepare a flat surface and fixed in position in a water tank during treatment with the laser lithotripter. The water tank is sufficiently large to ensure that the ambient water temperature near the stone surface does not vary drastically during the experiment (Supplementary Fig. S1).

The fiber was aligned perpendicularly (laser incident angle: 0°) and manually lowered to be in contact with the BegoStone surface. The delivery fiber attached to a strain gauge that would deflect when the fiber contacted the sample surface, and its reading was used to accurately set the fiber's axial position for each experiment (Fig. 1b). The stone samples were treated with a varying number of pulses (1–100 pulses, $n = 5$) at an output setting of 0.8 J and 10 Hz with the delivery fiber fixed in place. A customized user interface provided by Dornier was utilized to precisely control the number of pulses delivered per pedal hold.

High-speed videos were captured during the treatment, in which a light guide collecting the scattered laser light from

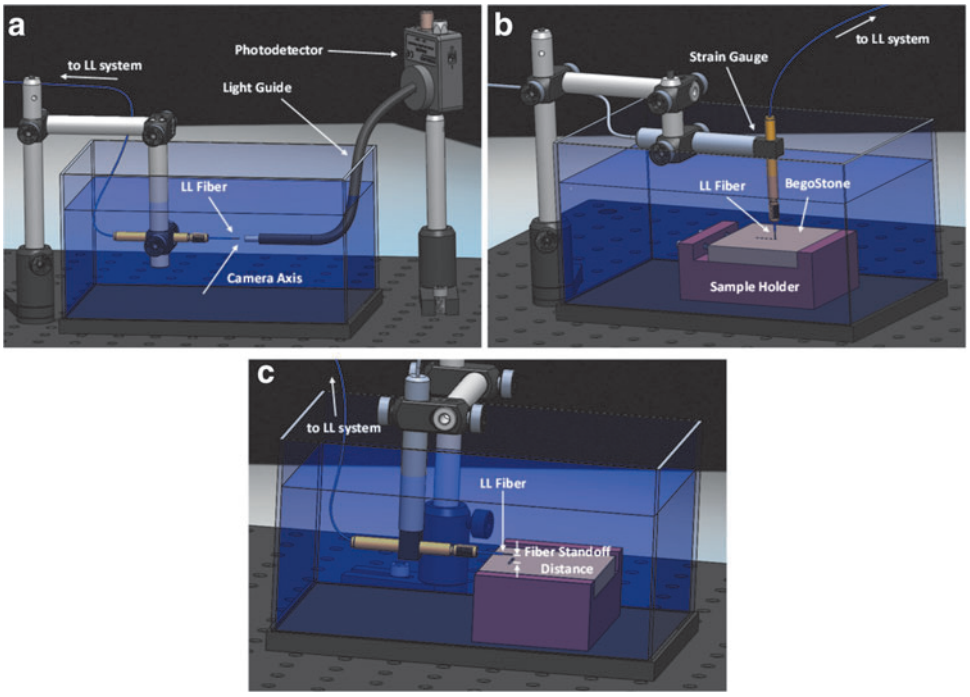

FIG. 1. Benchtop setup for **(a)** energy delivery measurements synced with high-speed imaging of bubble dynamics at the fiber tip, and BegoStone crater damage experiments with laser fiber aligned either **(b)** perpendicular or **(c)** in parallel to the stone surface.

the sample to a photodetector was used to trigger the camera from the first pulse. A digital time delay generator (BNC 565; Berkeley Nucleonics Corporation) was then used to trigger the camera to capture the cavitation event produced by each subsequent pulse from which the maximum bubble size was quantified. In addition, several human COM stones were cold mounted in an epoxy resin and polished before treatment by using Standard mode in water to verify the damage results obtained from BegoStone samples.

Stone damage was quantified by using optical coherence tomography (OCT), (OQ Labscope; Lumedica, Durham, NC). A custom software was developed in MATLAB (MathWorks, Natwick, MA) to map the depth of the stone surface and segment the crater region resulting from LL treatment. The volume, maximum depth, and area of the surface profile were quantified for each crater region. To investigate the effects of LL-induced bubble on stone damage, the experimental procedure was repeated in air with BegoStone and COM stone samples presoaked in water overnight. By treating the water-saturated stones in air, optical absorption by the intermediate fluid was removed, thus eliminating the damage contribution from the LL-induced bubbles while isolating the photothermal ablation effect within the sample. Cavitation-induced damage was analyzed by comparing the resultant craters from treatment in air *vs* in water.

Parallel fiber experiments for assessing effects of cavitation on stone damage

A set of experiments were conducted in both water and air with the fiber tip oriented parallel (laser incident angle: 90°) to the stone surface with the bottom of the fiber at a SD of 0.5, 1, and 2 mm (Fig. 1c). This orientation minimized light absorption by the stone and reduced the contribution of photothermal damage. Thus, parallel fiber experiments conducted in water isolated the damage caused by LL-generated cavitation whereas the experiments conducted in air served as a negative control (no photothermal or cavitation-induced damage). The stones were treated by using Standard mode (0.8 J, 10 Hz). After treatment of 1 to 100 pulses, the resultant crater volumes were quantified with OCT.

Stress fields resulting from LL bubble collapse were analyzed by using a previously developed photoelastic imaging system that has been used extensively to study transient stress fields.[21,22] Briefly, a photoelastic sample under stress becomes birefringent and causes a relative phase shift between the two polarization components of an incident light beam propagating along the two principal stress directions in the material. When combined outside the sample, the transmitted beam creates an interference fringe patterns that encode the transient stress field produced by a shock wave or jet impact from asymmetric bubble collapse, which can be captured by a high-speed camera. For illustration purpose, the laser fiber was oriented either perpendicular or parallel to a polyurethane block (PSM-4) at SD = 1–2 mm to avoid direct thermal damage of the material, and the transient stress fields produced in the block were recorded over the duration of bubble expansion and collapse after a single laser pulse.

Results

Pulse energy analysis

The normalized power profile over time for each pulse mode as measured in air and water is shown in Figure 2a–c. The corresponding high-speed image of the LL-generated bubble in water is shown above the graph. For all pulse modes, as the vapor bubble expands in water (thus shortening the distance between the tip of the bubble and the light guide or a stone surface), the energy transmission will increase gradually, reaching a peak between 150 and 200 μsec. In contrast, with minimal absorption of the Ho:YAG laser in air, the energy transmission will build up more rapidly with a peak achieved between 20 and 150 μsec. Further, no statistical differences were observed in relative pulse energies for the three treatment modes measured in air. However, a statistically significant increase in the energy delivered was observed in water for longer pulse durations (Fig. 2d–g).

OCT analysis of crater volume and geometry

Perpendicular fiber orientation. For all treatment modes in water, crater volumes increased drastically over the first 10 to 15 laser pulses before plateauing after about 20 pulses (Fig. 3a). During this treatment period, a similar increase and plateau in the LL bubble size was observed along with a transition in bubble dynamics from a small and flat pancake-shaped bubble to a round and large hemispherical bubble (Fig. 4).

The resultant crater volumes were higher for shorter pulse modes than those produced by longer pulse modes. Comparison of the crater profile area and depth (Fig. 3b, c) suggests that the larger crater volume in the shorter pulse mode was predominantly caused by the widening of the craters, whereas the average crater depths were comparable among different modes after 100 laser pulses. These differences along with the evolution of the crater over pulse number are displayed in the OCT reconstruction of representative crater volumes in Figure 5a–c. Further, the treatment of COM stones with standard mode pulses resulted in similar trends in damage progression with pulse number, whereas the plateaued crater volume and depth were found to be larger for COM stones than for BegoStone samples (Fig. 3a–c).

In addition, as a reference the crater volumes and geometry produced by a single pulse are shown in Supplementary Figure S2. However, the high variability in the pulse energy due to a feedback system for energy normalization within the lithotripter might increase uncertainty of these results.

In comparison to the stone damage produced in water, craters for BegoStones and COM stones treated with the same pulse modes in air exhibited dissimilar damage characteristics (Fig. 3d–f). In particular, crater volumes were lower for wet stones treated in air for all pulse modes. In addition, the crater depth for stones treated in water had a sharp plateau at $\sim$0.8 mm (Fig. 3b), whereas the crater depth for stones treated in air were deeper and still increasing after 100 laser pulses (Fig. 3e). On the other hand, the crater profile for stones treated in air were narrower compared with those for stones treated in water (Fig. 3f). These differences can be appreciated visually in the OCT reconstruction of representative BegoStone crater volumes for each pulse mode after treatment of 100 pulses (Fig. 5d–f). The ratio in crater volume and geometry between samples treated in water and air is shown in Supplementary Figure S3.

Parallel fiber orientation. The OCT reconstruction of the BegoStone surface after treatment in water with the parallel fiber exhibited a distinct crater pattern at each fiber SD from

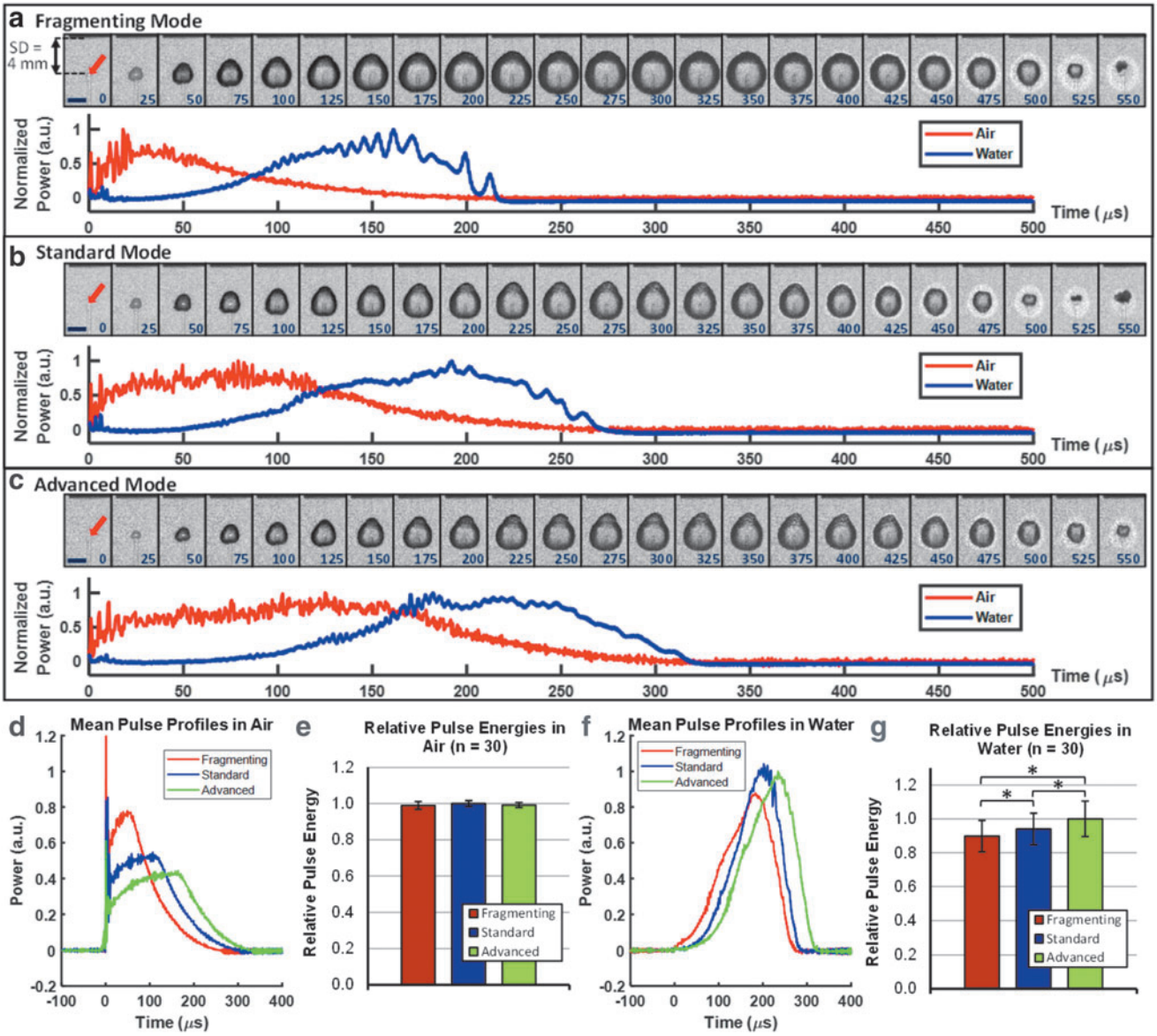

FIG. 2. Still frames from high-speed video of bubble expansion and collapse (corresponding time in microseconds shown in *blue*) for **(a)** fragmenting, **(b)** standard, and **(c)** advanced pulse modes (2 mm scale bar and *red arrow* marking fiber tip location in the 0 μsec frame). Plot of the normalized pulse power is shown below from photodetector measurements in air (*red*) and in water (*blue*) that were synced with the video frames above. The mean pulse power profiles for each mode and the relative energies between treatment modes measured in air **(d**, **e**, respectively**)** and through a light guide offset from the LL fiber by 4 mm in water **(f**, **g**, respectively). (*$p < 0.05$). LL = laser lithotripsy.

the stone. At SD = 0.5 mm, one crater was observed beneath the fiber tip and three craters $\sim$1 mm away. At SD = 1.0 mm, a similar crater pattern was produced with a lateral extension of the crater beneath the fiber. At SD = 2.0 mm, only in a single crater located beneath the fiber tip was observed (Fig. 6a).

High-speed imaging sequences of the LL bubble expansion and collapse were captured from both the side- and top view (Fig. 6b). Because of the significant elongation during expansion, the bubble collapsed asymmetrically and faster along the axial direction toward the fiber tip, breaking the bubble volume into two side lobes (SD = 0.5 mm) or leading to the formation of toroidal bubbles (SD = 1.0 mm) that collapsed afterward at a lateral distance from the fiber axis. The positions of the resultant craters correlated with the spots of bubble collapse, as confirmed by the dust plume ejected from the stone surface (see frames at 650 μsec in Fig. 6b). In addition, no craters were observed when treating the stone with a parallel fiber in air within the SD range of 0.5 to 2 mm, further suggesting that all the craters produced in water were caused by cavitation bubble collapse.

As shown in Figure 6c, crater damage was initiated after about 15 pulses and increased progressively thereafter toward 100 pulses for all SDs, which is in distinct contrast to the damage plateau produced by the perpendicular fiber orientation, in which a dominant photothermal effect is anticipated initially. The crater volume was found to increase from SD = 0.5 mm to 1.0 mm and then drop at 2.0 mm, indicating the existence of an optimal SD for cavitation-generated surface erosion. After 100

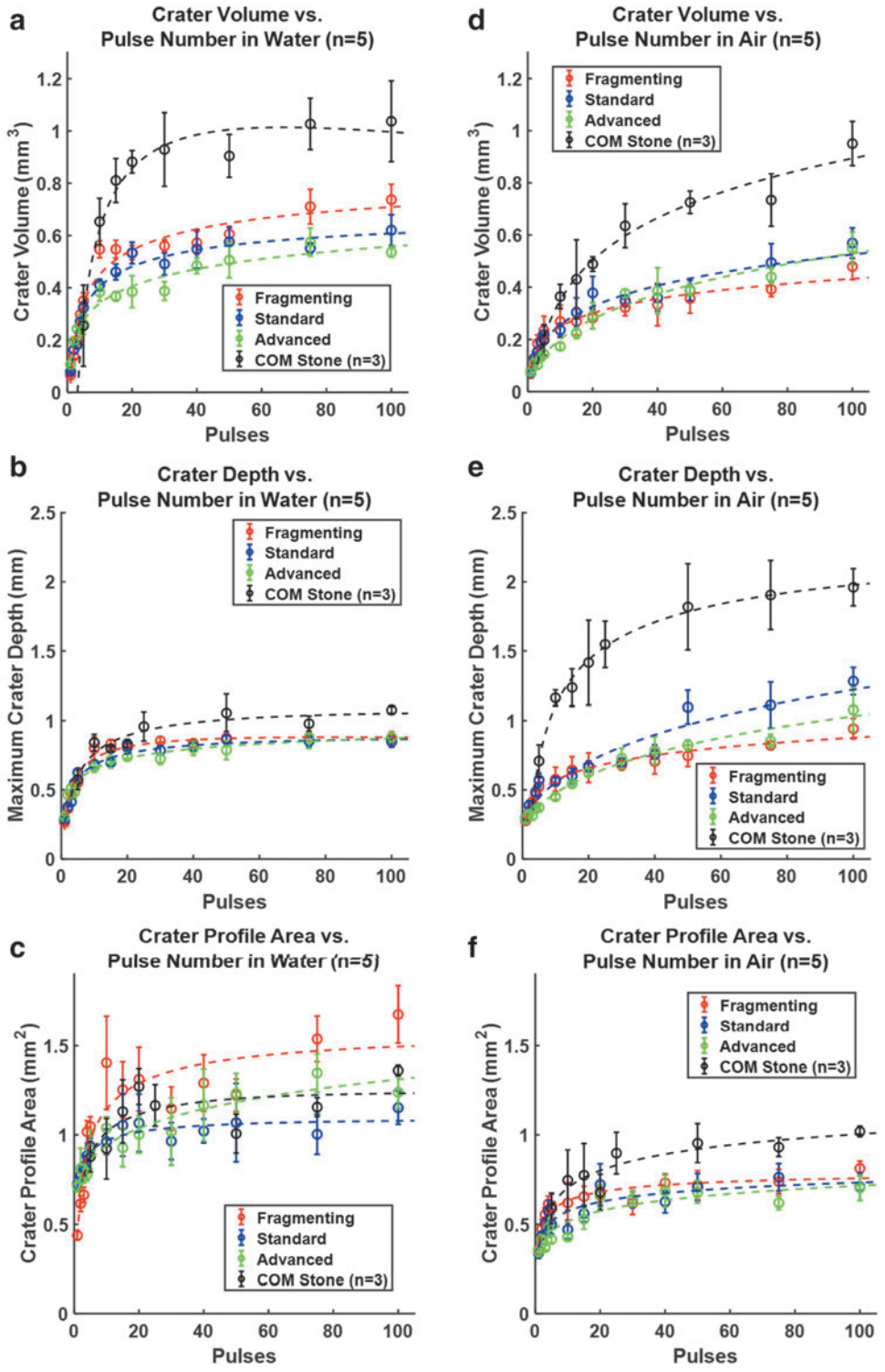

FIG. 3. Quantitative OCT analysis BegoStone and COM stone craters after LL treatment with the perpendicular fiber in contact with the stone surface (0.8 J and 10 Hz) in water **(e)** and in air **(d–f)** for 3 laser pulse modes from 1 to 100 pulses. Crater volume **(e, d)**, depth **(b, e)**, and surface profile area **(c, f)** are plotted on equivalent *y*-axis scales across treatment in water and air for comparison along with the logarithmic fits (*dotted lines*). OCT = optical coherence tomography.

pulses, a mean crater volume of 0.513 mm^3 was measured at SD = 1.0 mm, which corresponds to about 82.7% of the crater volume produced by the fiber in perpendicular orientation after the same number of pulses (Fig. 6d). Finally, photoelastic imaging demonstrated the generation of localized stress fields where the LL-induced bubble collapsed onto the substrate surface with the fiber oriented either perpendicular or parallel to the substrate (Fig. 6e, f).

Discussion

During Ho:YAG LL, rapid vaporization of fluid at the laser fiber tip results in the formation of an elongated vapor bubble, known as the Moses effect, which is conventionally believed to facilitate energy delivery and thus promote thermal ablation of the stone. Although the impact of pulse settings on stone retropulsion and treatment outcomes

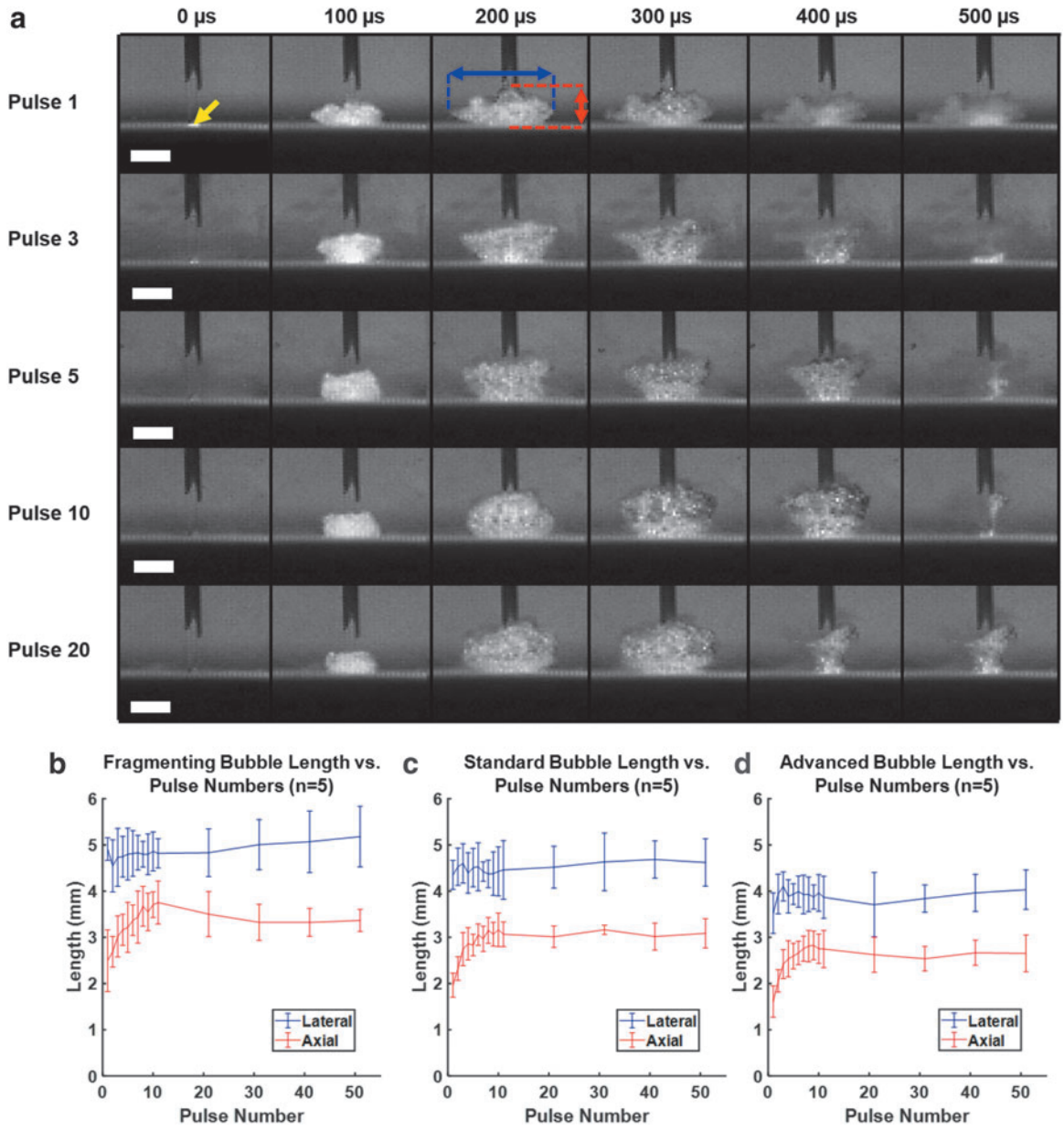

FIG. 4. **(a)** Representative high-speed imaging sequences of bubble dynamics by the standard mode pulses (scale bar = 2 mm, *yellow arrow* indicates fiber tip position). The lateral (*blue arrow*) and axial (*red arrow*) widths of the bubble (as marked in Pulse 1 at 200 μsec) were quantified for analysis. High-speed imaging analysis of bubble size for varying pulse number for **(b)** fragmenting, **(c)** standard, and **(d)** advanced modes operated at 0.8 J and 10 Hz.

has been previously investigated,[11,23] the contribution of the bubble to stone damage is poorly understood. In this work, we present striking evidence supporting a direct contribution of LL-induced bubble collapse as a secondary mechanism of stone damage that occurs in conjunction with the dominant photothermal mechanism widely recognized in the literature.[6,7] This new finding suggests that future development of laser technology and pulse modulation strategy should consider optimization of bubble dynamics during LL to improve stone fragmentation.

Photodetector measurements demonstrate that the vapor bubble will improve energy delivery to the stone surface for longer pulse modes because a greater proportion of the laser pulse is transmitted to the stone after the formation of the vapor bubble (Fig. 2). This finding is consistent with the basis of ''Moses™ Technology'' (Lumenis, Yokneam, Israel), whereby a portion of the pulse energy is delivered after the formation of the vapor bubble, giving rise to improved energy delivery and an increase in photothermal damage.[11,13,23,24] In the perpendicular fiber experiments, the MOSES effect is anticipated to improve energy delivery to the stone as the crater forms and the fiber-stone distance increases. However, despite the higher energy delivery, stone damage and crater depth were not improved for the longer pulse modes after 15 pulses (Fig. 3). This observation is consistent with previous studies that demonstrated either no improvement or less stone damage with longer pulses.[2–4,23,25]

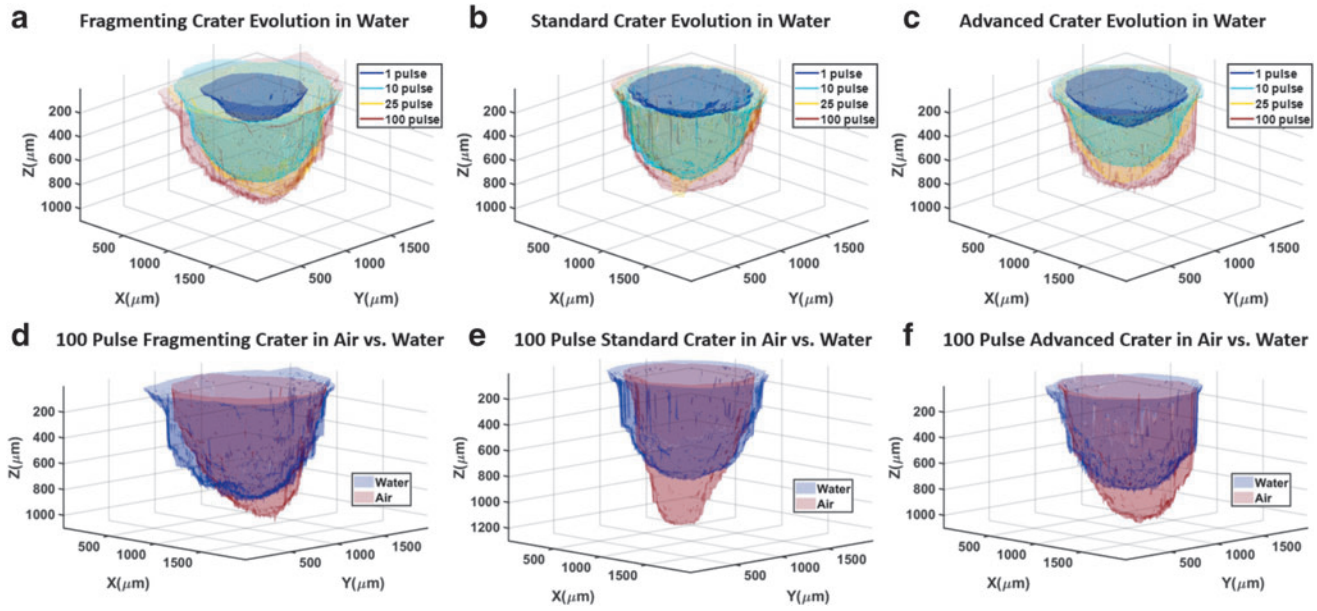

FIG. 5. **(a–c)** Examples of OCT 3D reconstruction of characteristic crater evolution for LL treatment of BegoStone samples after different pulses and **(d–f)** for comparison of damage crater profiles produced after 100 pulses in water *vs* in air using the three pulse modes operated at 0.8 J and 10 Hz.

A careful evaluation of the crater volume change with pulse number (Fig. 3a) suggests a multiphase process of stone damage during LL: from (1) an initial rapidly growing phase (1 to 10 pulses) in which photothermal effect may be dominant, to (2) a transition phase (10 to 40 pulses) in which cavitation-induced damage may become progressively important, to eventually (3) the plateau phase (40 and beyond) in which continued delivery of the laser energy yields a diminished return in stone damage. Specifically, in the transition phase when the crater depth (and thus the fiber-stone distance) increased rapidly to >0.5 mm after the initial 10 pulses (Fig. 3b), more laser energy is absorbed by the intermediate fluid with a concomitant increase in bubble size (Fig. 4b) and as a result, less energy is delivered to the target stone. Thereafter, damage craters slowly reached a plateau independent of the pulse modes (Fig. 3b). A similar trend in plateauing damage with increasing pulse number was also observed recently by Aldoukhi et al.[26]

In comparison, without significant laser energy loss due to bubble formation, the damage craters produced in wet stone samples treated in air showed progressively increasing crater depth (Fig. 3e), with similar yet narrow surface profile areas among different pulse modes (Fig. 3f). This is in distinct contrast to damage craters for stones treated in water that plateaued in crater depth (Fig. 3b) yet exhibited broader surface profile areas with high variation between pulse modes (Fig. 3c).

The variation in crater geometry between stones treated in air *vs* in water suggests that cavitation plays a significant role in the widening of craters. In particular, the shorter (i.e., fragmenting) pulse mode with its high peak power (Fig. 2d) was found to produce larger bubbles (Fig. 4b–d) and resulted in greater crater surface profile areas and crater volume than its counterpart longer (i.e., standard and advanced) pulse modes (Fig. 3a, c). It is likely that higher laser energy absorption in the intermediate fluid by the shorter pulse mode will result in a larger cavitation bubble and thus greater stress concentration and erosion damage produced on the stone surface by the asymmetric collapse of the bubble with microjet impact.[27] Overall, we hypothesize that photothermal ablation and microexplosion mechanisms play a dominant role in controlling the crater depth whereas cavitation bubble collapse contributes significantly to the broadening of the crater surface area and thus damage volume. Future studies are warranted to further dissect this complex process.

Moreover, the contribution of cavitation to stone damage in LL is demonstrated unambiguously by the results from the parallel fiber experiments in water. At sufficiently large SD (≥0.5 mm), no photothermal damage was produced by treating wet stones in air whereas significant crater formation with damage pattern consistent with bubble collapse was produced in water (Fig. 6). Although some photothermal damage might be anticipated in treatment with a parallel fiber due to potential lensing effect from the vapor bubble, this highly dynamic process is unlikely to generate the reproducible crater patterns observed in the experiments.

More importantly, as the SD increased from 0.5 to 1.0 and further to 2.0 mm, the crater damage would first increase and then drop in contradiction to the expectation from photothermal ablation mechanism. Further, detectable crater damage was only observed after about 15 to 20 pulses, indicating that repeated bombardments from the microjet impact of bubble collapse are required to initiate cavitation damage. This feature is in contrast to the immediate stone damage produced by photothermal ablation when the fiber was placed perpendicularly in contact with the stone surface. In addition, the crater depth produced by cavitation erosion in parallel fiber orientation was shallower, yet with greater surface profile area (accumulated from multiple spots of toroidal bubble collapse) than the counterpart produced by photothermal ablation in combination with cavitation damage in the perpendicular fiber orientation (Fig. 6a). The trajectory in crater volume *vs* pulse number curves also varies drastically between these 2

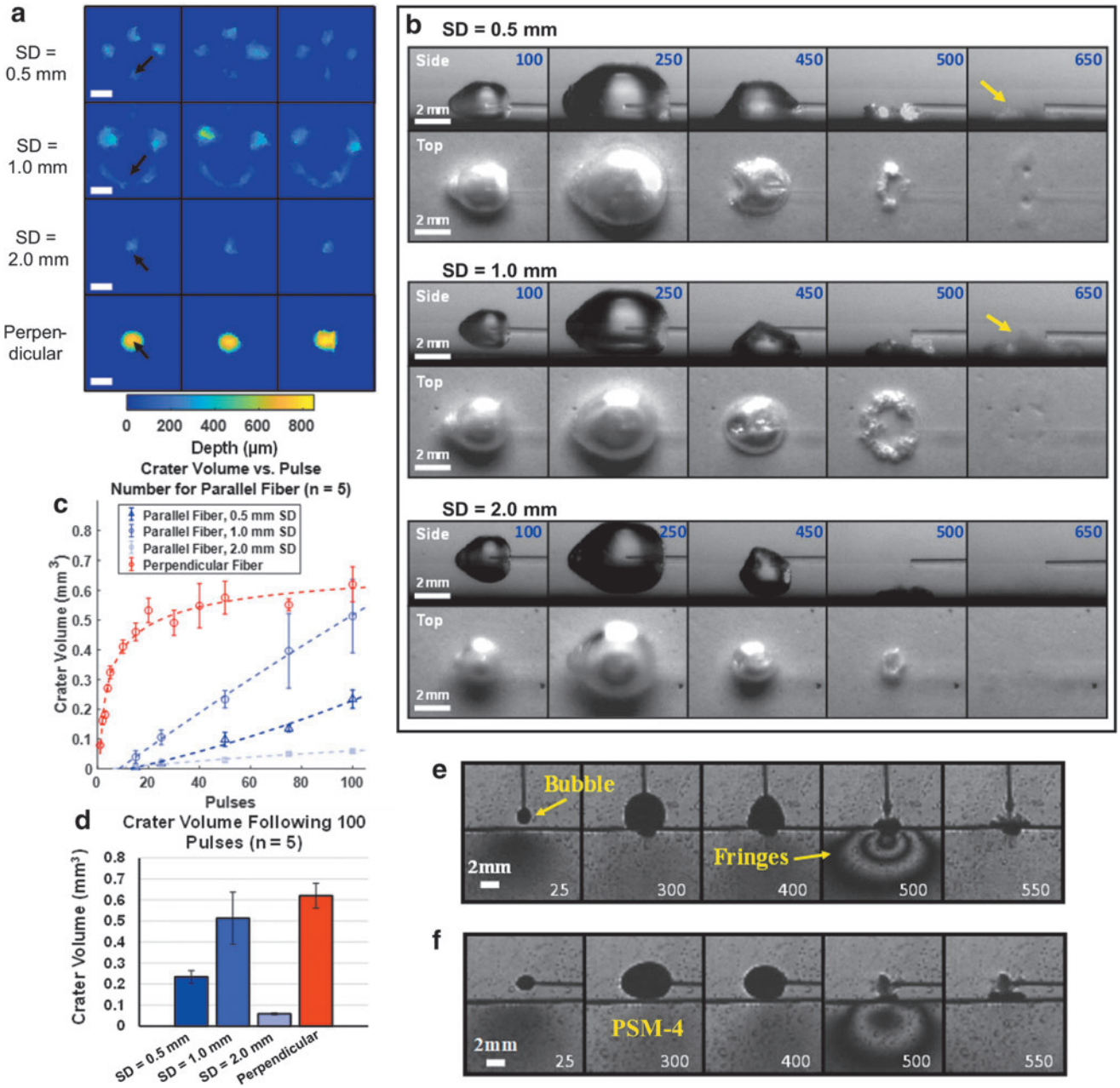

FIG. 6. **(a)** Three representative examples of OCT reconstruction of BegoStone sample surface after treatment with the parallel fiber at each of the three different SDs and using the perpendicular fiber in contact with the stone surface (*black arrows* indicate the fiber location, 1 mm scalebar). **(b)** Side- and top view of the bubble expansion and collapse. *Yellow arrow* indicates dust plume after the collapse of the bubble, and the time from the start of the pulse is shown in *blue*. **(c)** Cavitation-induced crater volumes over 100 pulses of parallel fiber treatment and **(d)** comparison of the crater volume after 100 pulses. The crater volume for equivalent treatment with a perpendicular fiber is shown for comparison (*red*). Photoelastic imaging for treatment with the fiber **(e)** perpendicular and **(f)** parallel to the substrate surface (corresponding time in microseconds shown in *white*). Fringes in the photoelastic images suggest that stress fields are produced by the bubble collapse. SD = standoff distance.

fiber orientations, with 1 plateauing after 20 pulses (i.e., perpendicular) and the other increasing steadily up to 100 pulses (i.e., parallel). Altogether, these new observations suggest that although photothermal damage is a dominant mechanism for stone damage in fragmentation mode at 0.8 J pulse energy, secondary cavitation effects can contribute significantly to the overall stone fragmentation process during LL. At the high pulse energy levels used in the fragmenting mode, the most efficient treatment is produced by placing the fiber perpendicular and in close proximity to the stone. It should be noted that the parallel fiber orientation is inadvisable for clinical LL in general due to the risk of tissue damage, except in inevitable cases during pop-dusting.

Asymmetric bubble collapse near a solid boundary is well known to cause the formation of a fluid jet toward the solid boundary (Supplementary Fig. S4).[6,15–18] Pressure transient

measurements did not detect a shockwave emission at the initial expansion, yet weak pressure pulses of increasing magnitude with shorter pulse width were detected during the collapse of the elongated bubble and its subsequent rebound (Supplementary Figs. S5 and S6).

Jet impact with resultant water hammer pressure created by the asymmetric bubble collapse is a complex process that is highly dependent on the bubble size, geometry, and proximity of the bubble to the stone surface.[28–30] The parallel fiber experiments demonstrate that the degree of cavitation damage is highly dependent on the fiber tip-stone separation distance and can be optimized only within a tight range. This offers an explanation to previous parallel fiber experiments that produced minimal damage,[6] and to the discrepancies in previous studies that have reported both improvements and reduction in stone damage with increasing SDs for varying pulse modes and energies,[6,23,31] Further systematic studies are needed to better understand cavitation-induced stone damage in LL as a function of both the laser pulse parameters and SD.

Some of the previous studies comparing Ho:YAG LL fragmentation of COM stones in water and air have shown higher mass loss for samples treated in air,[6,7] whereas others found no significant difference using BegoStones.[32] The discrepancies between previous studies and our results may be caused by the differences in the experimental setup and treatment protocols. For example, the fiber was scanned to maintain contact with the sample during treatment in the previous studies, which reduced the laser absorption by the fluid and at each spot on the sample, thus diminishing the cumulative effects of cavitation damage from repeated treatment in the same region as shown in the parallel fiber experiments.

Nevertheless, our observation of damage plateau highlights the importance of continuous repositioning of the fiber to maintain proper contact with the stone surface. With the advent of modern holmium lithotripters that offer high-frequency treatment modes (>80 Hz), a plateau in damage may occur in only a fraction of a second, which would require the development of automated schemes to optimize fiber scanning speed for improved fragmentation efficiency during LL.[33] It is also important to note, with the increased number of pulses fired in high-frequency ''dusting'' modes, the total cavitation events will greatly increase during a single LL procedure, which may further accentuate the effects of cavitation on stone damage.

As with all benchtop models, the current study is limited in simulating clinical conditions. Primarily, the fixed sample model neglects the effect of stone retropulsion on damage efficiency and introduces confounding factors such as debris shielding, which may absorb a portion of the laser energy and thereby lower fragmentation as observed during SWL.[34] In addition, the experiments were performed in an open tank, whereas an enclosed system, such as in the ureter or kidney calix, may alter the bubble dynamics.

In addition, the optical properties of BegoStones compared with kidney stones are not well characterized. Although spectroscopic measurements have previously been obtained on artificial and human kidney stones, they do not represent the optical absorption coefficients of the stone materials.[35,36] As observed in this study, COM stones craters were deeper and larger craters compared with BegoStones, suggesting higher optical absorption. Thus, the degree in which cavitation plays a role in stone damage may vary with human kidney stones of various compositions.

To address these limitations, future studies may be performed in a ureter or kidney model using human stones to determine how cavitation affects stone retropulsion and fragmentation and overall treatment efficiency. The pulse widths in this study were limited by the capability of the clinical lithotripter used. Further studies may investigate the cavitation damage produced in Hol:YAG lithotripsy at long pulses (>500 μsec). Finally, this study utilized high-energy (0.8 J) pulses in the LL ''fragmentation'' regime. Additional studies may investigate the damage induced by cavitation at lower pulse energies (0.2 J) to investigate the extent of cavitation-induced damage in the LL ''dusting'' regime and the contribution of cavitation to the characteristic differences in stone fragment sizes in these two treatment regimes.[37] These additional experiments may further elucidate the best potential avenue of pulse mode optimization to improve treatment efficiency during clinical LL.

Conclusions

Cavitation bubble dynamics represent a complex process that contributes significantly to the clinical efficacy of LL. Although recent LL technologies have included developments to improve stone fragmentation, the basic understanding of the role of cavitation during treatment has remained relatively stagnant.

This study presents new findings on how the LL bubble affects the efficiency of stone fragmentation during treatment and may constitute a secondary mechanism of stone damage, in addition to the well-recognized photothermal ablation and microexplosion damage mechanism. In particular, although longer pulse durations result in greater laser energy delivery to the stone, the resulting crater volume remains significantly smaller than those produced by shorter pulse durations. This finding along with the supporting evidence from the parallel fiber experiments demonstrate that cavitation-induced damage plays an essential role during LL treatment. Thus, strictly focusing on laser energy delivery efficiency and photothermal effects will neglect a substantial area of potential optimization. Future development of LL pulse modes should consider the effects of cavitation to improve the overall fragmentation efficiency of the system.

Acknowledgment

The authors would also like to express their gratitude to Dornier MedTech for providing the H Solvo laser used in this study.

Disclaimer

The content is solely the responsibility of the authors and does not necessarily represent the official views of the American Urological Association (AUA) or the Urology Care Foundation.

Author Disclosure Statement

G.M.P. serves as a consultant for Boston Scientific. M.E.L. serves as a consultant for Boston Scientific and Lumenis.

Funding Information

This project is supported by the National Institute of Health (NIH) through grants P20 DK123970 and R37 DK052985. D.S.H. is supported by the NIH (K12

DK100024). R.S.T. is supported by the Urology Care Foundation Research Scholar Award Program and AUA Southeastern Section.

Supplementary Material

Supplementary Figure S1
Supplementary Figure S2
Supplementary Figure S3
Supplementary Figure S4
Supplementary Figure S5
Supplementary Figure S6

References

1. Turk C, Petrik A, Sarica K, et al. EAU guidelines on interventional treatment for urolithiasis. Eur Urol 2016;69: 475–482.
2. Bader MJ, Pongratz T, Khoder W, et al. Impact of pulse duration on Ho:YAG laser lithotripsy: Fragmentation and dusting performance. World J Urol 2015;33:471–477.
3. Sroka R, Pongratz T, Scheib G, et al. Impact of pulse duration on Ho:YAG laser lithotripsy: Treatment aspects on the single-pulse level. World J Urol 2015;33:479–485.
4. Kang HW, Lee H, Teichman JM, Oh J, Kim J, Welch AJ. Dependence of calculus retropulsion on pulse duration during Ho: YAG laser lithotripsy. Lasers Surg Med 2006;38:762–772.
5. Finley DS, Petersen J, Abdelshehid C, et al. Effect of holmium:YAG laser pulse width on lithotripsy retropulsion in vitro. J Endourol 2005;19:1041–1044.
6. Chan KF, Vassar GJ, Pfefer TJ, et al. Holmium:YAG laser lithotripsy: A dominant photothermal ablative mechanism with chemical decomposition of urinary calculi. Lasers Surg Med 1999;25:22–37.
7. Vassar GJ, Chan KF, Teichman JM, et al. Holmium: YAG lithotripsy: Photothermal mechanism. J Endourol 1999;13: 181–190.
8. Fried NM. Recent advances in infrared laser lithotripsy [Invited]. Biomed Opt Express 2018;9:4552–4568.
9. Shalini S, Frank DS, Aldoukhi AH, et al. Assessing the role of light absoprtion in laser lithotripsy by isotopic substitution of kidney stone materials. ACS Biomater Sci Eng 2020;6:5274–5280.
10. Asshauer T, Rink K, Delacretaz G. Acoustic transient generation by holmium-laser-induced cavitation bubbles. J Appl Phys 1994;76:5007–5013.
11. Elhilali MM, Badaan S, Ibrahim A, Andonian S. Use of the Moses technology to improve holmium laser lithotripsy outcomes: A preclinical study. J Endourol 2017;31:598–604.
12. Mullerad M, Aguinaga JRA, Aro T, et al. Initial clinical experience with a modulated holmium laser pulse-Moses technology: Does it enhance laser lithotripsy efficacy? Rambam Maimonides Med J 2017;8:e0038.
13. Aldoukhi AH, Roberts WW, Hall TL, Ghani KR. Holmium laser lithotripsy in the new stone age: Dust or bust? Front Surg 2017;4:57.
14. Jansen ED, Asshauer T, Frenz M, Motamedi M, Delacretaz G, Welch AJ. Effect of pulse duration on bubble formation and laser-induced pressure waves during holmium laser ablation. Lasers Surg Med 1996;18:278–293.
15. Lindau O, Lauterborn W. Investigation of the counterjet developed in a cavitation bubble that collapses near a rigid boundary. In: Proceedings of the Fourth International Symposium on Cavitation, Pasadena. 2001:A5.001.
16. Bolle H, Lauterborn W. Experimental investigations of cavitation-bubble collapse in the neighbourhood of a solid boundary. J Fluid Mech 1975;72:391–399.
17. Plesset MS, Chapman RB. Collapse of an initially spherical vapour cavity in the neighbourhood of a solid boundary. J Fluid Mech 1971;47:283–290.
18. Rudhart M, Hirth A. Use of an absorbent in laser lithotripsy with dye lasers: In vitro study of fragmentation efficiency and jet formation. J Urol 1994;152:1005–1008.
19. Esch E, Simmons WN, Sankin G, Cocks HF, Preminger GM, Zhong P. A simple method for fabricating artificial kidney stones of different physical properties. Urol Res 2010;38:315–319.
20. Simmons WN, Cocks FH, Zhong P, Preminger G. A composite kidney stone phantom with mechanical properties controllable over the range of human kidney stones. J Mech Behav Biomed Mater 2010;3:130–133.
21. Xi X, Zhong P. Dynamic photoelastic study of the transient stress field in solids during shock wave lithotripsy. J Acoust Soc Am 2001;109:1226–1239.
22. Maxwell AD, MacConaghy B, Bailey MR, Sapozhnikov OA. An investigation of elastic waves producing stone fracture in burst wave lithotripsy. J Acoust Soc Am 2020;147:1607.
23. Aldoukhi AH, Roberts WW, Hall TL, Ghani KR. Watch your distance: The role of laser fiber working distance on fragmentation when altering pulse width or modulation. J Endourol 2019;33:120–126.
24. Ibrahim A, Fahmy N, Carrier S, Elhilali M, Andonian S. Double-blind prospective randomized clinical trial comparing regular and Moses modes of holmium laser lithotripsy: Preliminary results. J Urol 2018;199:E1047-E.
25. Wezel F, Hacker A, Gross AJ, Michel MS, Bach T. Effect of pulse energy, frequency and length on holmium: yttrium-aluminum-garnet laser fragmentation efficiency in non-floating artificial urinary calculi. J Endourol 2010;24:1135–1140.
26. Aldoukhi AH, Black KM, Hall TL, Roberts WW, Ghani KR. Frequency threshold for ablation during holmium laser lithotripsy: How high can you go? J Endourol 2020; 34:1075–1081.
27. Plesset MS, Ellis AT. On the mechanism of cavitation damage. Trans ASME 19555;77:1055–1064.
28. Blake JR, Gibson DC. Cavitation bubbles near boundaries. Ann Rev Fluid Mech 1987;19:99–123.
29. Lauterborn W, Kurz T. Physics of bubble oscillations. Rep Prog Phys 2010;73:106501.
30. Philipp A, Lauterborn W. Cavitation erosion by single laser-produced bubbles. J Fluid Mech 1998;361:75–116.
31. De Coninck V, Keller EX, Chiron P, et al. Ho:YAG laser lithotripsy in non-contact mode: Optimization of fiber to stone working distance to improve ablation efficiency. World J Urol 2019;37:1933–1939.
32. Taratkin M, Laukhtina E, Singla N, et al. How lasers ablate stones: In vitro study of laser lithotripsy (Ho:YAG and Tm-Fiber Lasers) in different environments. J Endourol 2020. [Epub ahead of print]; DOI: 10.1089/end.2019.0441.
33. Hall LA, Gonzalez DA, Fried NM. Thulium fiber laser ablation of kidney stones using an automated, vibrating fiber. J Biomed Opt 2019;24:1–10.
34. Randad A, Ahn J, Bailey MR, et al. The impact of dust and confinement on fragmentation of kidney stones by shockwave lithotripsy in tissue phantoms. J Endourol 2019;33:400–406.
35. Chan KF, Choi B, Vargas G, et al. Free electron laser ablation of urinary calculi: An experimental study. IEEE J Sel Top Quantum Electron 2001;7:1022–1033.

36. Frank DS, Aldoukhi AH, Roberts WW, Ghani KR, Matzger AJ. Polymer-mineral composites mimic human kidney stones in laser lithotripsy experiments. ACS Biomater Sci Eng 2019;5:4970–4975.
37. Sea J, Jonat LM, Chew BH, et al. Optimal power settings for Holmium:YAG lithotripsy. J Urol 2012;187:914–919.

Address correspondence to:
Derek S. Ho, PhD
Department of Mechanical Engineering
and Materials Science
Duke University
Durham, NC 27705
USA

E-mail: derek.ho@duke.edu

Pei Zhong, PhD
Department of Mechanical Engineering
and Materials Science
Duke University
Durham, NC 27705
USA

E-mail: pzhong@duke.edu

Abbreviations Used

COM = calcium oxalate monohydrate
LL = laser lithotripsy
OCT = optical coherence tomography
SD = standoff distance
SWL = extracorporeal shockwave lithotripsy